International Journal of Solids and Structures 50 (2013) 3911–3921

Contents lists available at ScienceDirect

International Journal of Solids and Structures

journal homepage: www.elsevier.com/locate/ijsolstr

Influence of softening on fracture propagation in large-scale shell structures

M. Kõrgesaar *, J. Romanoff

Aalto University, School of Engineering, Department of Applied Mechanics, P.O. Box 15300, FIN-00076 Aalto, Finland

ARTICLE INFO

Article history:
Received 27 April 2013
Received in revised form 1 July 2013
Available online 7 August 2013

Keywords:
Large structures
Softening
Shell elements
Ductile fracture
Finite elements

ABSTRACT

In this study, fracture propagation in large shell elements is modelled with the softening law. This law is given in a general form, enabling investigations of different softening behaviours to be conducted. The final fracture is simulated by removing elements. The softening parameters are derived using the energy-based representative volume element (RVE) approach. Tracing crack propagation through the RVE defines the physically justified softening parameters for the current model. The softening model is implemented into ABAQUS using VUMAT subroutines for the shell elements. A large-scale tearing experiment is simulated with the current model and RVE-based softening parameters. In addition, the softening laws from the literature have been used. The fracture propagation is assessed in terms of plastic energy dissipation in the RVE and the whole structure, load–displacement, and crack growth. The RVE-based model is shown to have better performance compared with other models from the literature.

1. Introduction

The structural safety of large-scale thin-walled structures has become more important as a result of the increased societal awareness regarding accidents and structural failure. The failures can happen because of collisions, explosions, fatigue-induced damage, and the overloading of the structure by forces of nature, which do not have a clear upper bound. A fracture in a thin-walled structure can lead to the leakage of gases and liquids, endangering the environment and human lives. Therefore, fracture propagation is of the utmost importance in large-scale structures, such as ships, bridges, offshore structures etc. When the structures being analysed become large, detailed modelling of the fracture process becomes prohibitive, considering current software and hardware capabilities. The present paper is concerned with simulating a ductile fracture with large shell elements where the element length is at least the thickness of the plate. In general, there are two main approaches to model fracture in large-scale shell structures: sudden fracture criteria and Continuum Damage Mechanics (CDM) (Jones, 2013). According to sudden fracture criteria, elements are removed from the simulation once the critical stress–strain state has been reached; see Fig. 1. These criteria usually depend on the rupture strain (Yamada et al., 2005; Simonsen and Törnqvist, 2004), which is often adjusted on the basis of stress triaxiality (Li et al., 2011; Törnqvist, 2003; Bao and Wierzbicki, 2004a). However, the effect on constitutive equations is ignored, meaning that the fracture model and material model are uncoupled. Consequently, crack propagation is a discontinuous event, which introduces process and structural discontinuities due to the sudden deletion of shell elements. In CDM, an attempt is made to remove this process discontinuity by coupling of the constitutive model and fracture model. There, the fracture is described as a continuous degradation of material strength with an internal variable called damage (Chaboche, 1981; Lemaitre, 1985). Damage represents on a macro scale the reduction of the effective load-carrying area in the material caused by microcracks and voids. Recently, several authors have modified the approach by introducing damage directly to the hardening curve (Xue, 2007; Teng, 2008; Li and Wierzbicki, 2010), resulting in a softened flow stress compared with the original undamaged flow stress; see Fig. 1.

In Fig. 1, the area under softened part of the flow curve corresponds to the strain energy needed to propagate crack through the element. If the element size is small ($L_e \ll$ size of the local neck), the most of the deformation energy is consumed before the fracture initiation and standard flow curve without softening can successfully describe the material behaviour. For example, according to the relation of Li and Wierzbicki (2010), there is a sudden discontinuity at the point of fracture initiation; see Fig. 1. Hence softening is only necessary to predict slant fracture in plane strain specimens (Besson, 2010; Li and Wierzbicki, 2010; Gruben et al., 2012). In this case, material damage begins when fracture initiates as denoted in Fig. 1. However, in the analyses with large shell elements, the point of fracture initiation and the processes leading to that, such as necking, must be described in the average sense. In the context of large shell elements, the term (fracture)

* Corresponding author. Tel.: +358 505648878; fax: +358 947024173.
E-mail address: mihkel.korgesaar@aalto.fi (M. Kõrgesaar).

0020-7683/$ - see front matter © 2013 Elsevier Ltd. All rights reserved.
http://dx.doi.org/10.1016/j.ijsolstr.2013.07.027

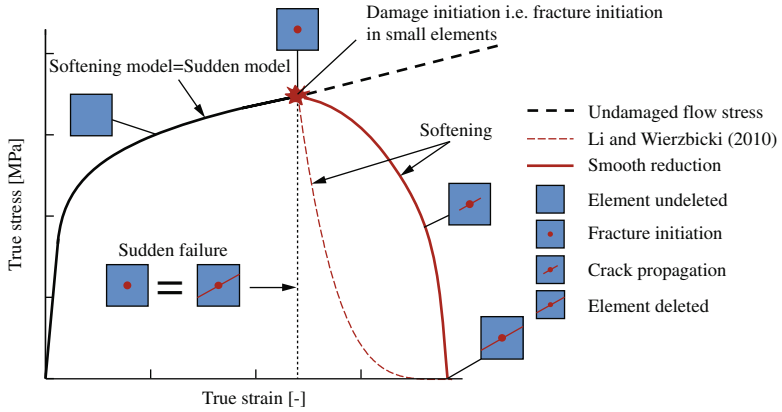

Fig. 1. Sudden fracture criterion and different softening approaches in small elements ($L_e \ll$ size of the local neck).

initiation is used throughout the paper to describe the setting where propagating crack reaches an element. In other words, only fracture propagation is considered. Alsos et al. (2008) argue that large shell elements cannot capture the onset of necking and strain-softening taking place before fracture. However, Woelke and Abboud (2012) showed that this limitation can be removed by the smooth reduction of flow stress beyond necking. In that way, averaging the fracture processes over a large area eliminates the discontinuity at fracture initiation. Their model is calibrated on the basis of a tensile test. In a different study, tensile tests were again used to calibrate the bilinear softening relation (Hogström et al., 2009). Later, they applied this relation to simulate ship collision damage (Hogström and Ringsberg, 2012). AbuBakar and Dow (2013) adopted linear softening beyond fracture initiation to simulate ship grounding damage, but no justification for the linear relation was given. Thus, softening parameters for large elements are commonly calibrated from tensile tests where only the point of fracture initiation is captured, or they are implicitly assumed. How this influences fracture propagation analyses, and thus the crashworthiness analyses of structures, is unknown.

This paper presents a numerical method to predict the softening parameters for shell elements and studies the influence of softening on fracture propagation in large structures. First, in Section 2, a softening model is introduced in which damage-induced softening is separated into two stages. Formulation is carried out in a way that mathematical treatment of different softening laws can be performed (Li and Wierzbicki, 2010; Hogström et al., 2009; AbuBakar and Dow, 2013). Consideration of an averaging unit in the neighbourhood of the crack tip, where the dissipated energy is calculated using solid elements, defines the characteristics of the fracture process, and thus the softening parameters. The approach is validated by the plate tearing tests of Simonsen and Törnqvist (2004) in Section 3. The results are discussed in Section 4 and the study is concluded in Section 5. Study is limited to Mode I type of fracture. The fracture initiation is not addressed and focus is on relatively large amounts of crack extension. For long cracks, Mode I dominates and stress stated ahead of the tip is fully established with uniaxial tension as the prevailing mechanism (Tvergaard and Hutchinson, 1992).

2. Formulation of the softening model

2.1. Model description

Onset of necking is understood as the bifurcation from an uniform deformation mode, which in the Considère sense occurs when the maximum force is reached in a simple tension bar. In the current model softening begins with the formation of neck and continues smoothly until the point of fracture initiation. This captures the strain softening beyond necking and is denoted as the 1st softening stage in Fig. 2(a). After initiation, fracture starts to propagate, which in an average sense must be captured with large shell elements. Fracture propagation is denoted as the 2nd softening stage in Fig. 2(a), where stress reduction is significant for the increasing strain. Treating fracture propagation as a separate stage is in alignment with stable ductile crack growth under extensive plastic deformation. For instance, a single large element mapped to the crack path in Fig. 2(b) must capture the physical processes described in Fig. 2(c).

2.2. Damage evolution

Before the fracture initiation softening is induced by the damage D_1 and after the fracture initiation by the damage D_2; see Fig. 2(a). The damage D_1 is proportional to the equivalent plastic strain $\bar{\varepsilon}^p$. It is normalised in such a way that $D_1 = 1$ once the condition for a diffuse neck according to the Considère conditions is satisfied; for details see Appendix A:

$$D_1 = \frac{\int d\bar{\varepsilon}^p}{n} = \frac{\bar{\varepsilon}^p}{n}, \tag{1}$$

where n is the strain hardening exponent. The damage D_2 specifies the point of fracture initiation at $D_2 = 1$ and describes the fracture propagation stage:

$$D_2 = \int_0^{\bar{\varepsilon}^p} \frac{\mathrm{d}\bar{\varepsilon}^p}{\bar{\varepsilon}_f^p(\eta_{av})}, \tag{2}$$

where η_{av} the average stress triaxiality, and $\bar{\varepsilon}_f^p(\eta_{av})$ a fracture locus in the space of equivalent plastic strain and stress triaxiality. The stress triaxiality is: $\sigma_h/\bar{\sigma}$, where the equivalent stress is $\bar{\sigma} = \sqrt{3J_2}$; J_2 is the second invariant of the deviatoric stress tensor and σ_h is the hydrostatic stress.

2.3. Softening

When softening is considered two different flow curves are distinguished; see Fig. 2(a). The original true stress–strain relation of the undamaged material determined with a tensile test and the softened curve. Undamaged material is described with the equivalent stress, i.e. $\bar{\sigma} = \bar{\sigma}(\bar{\varepsilon}_p)$. The softened flow stress $\tilde{\sigma}$ is introduced by considering the damage evolution beyond critical damage:

$$\tilde{\sigma} = \beta\bar{\sigma}, \tag{3}$$

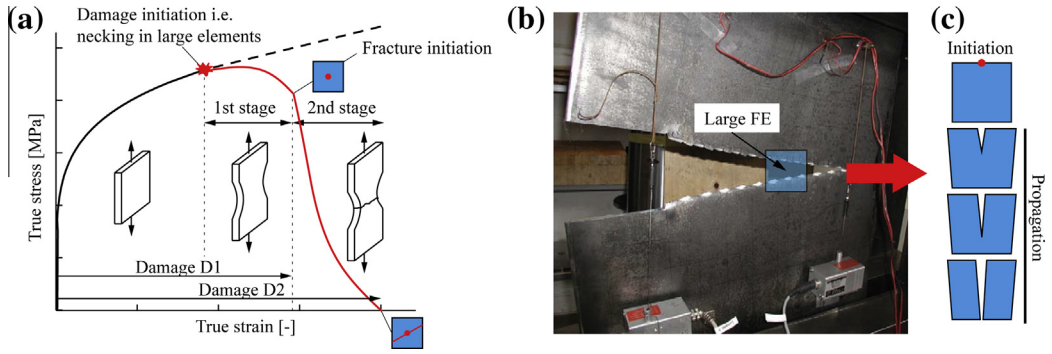

Fig. 2. (a) Illustration of two-stage softening model. (b) Tearing of a large plate. Background figure from Simonsen and Törnqvist (2004). (c) Physical behaviour that must be captured in an average sense by a single large finite element.

where β is the softening coefficient that is a function of damage. Softening begins when $\beta = 1$ and crack has propagated through the element when $\beta = 0$. The strain evolution does not require any modification because of the hypothesis of strain equivalence (Lemaitre, 1985): the strain in the softened material is assumed to be equal to that in the undamaged material.

The softening coefficient β is calculated as

$$\beta = \beta_1(D_1) \cdot \beta_2(D_2), \tag{4}$$

where β_1 is the softening induced by D_1 and β_2 is the softening induced by D_2. Again, the two softening coefficients ($\beta_{1,2}$) range from 1 to 0, which for both stages are calculated with the same expression:

$$\beta_1, \beta_2 = \left(\frac{D_c - D}{D_c - D_0}\right)^m, \tag{5}$$

where D_c, D_0 and m are softening parameters. Without splitting softening into two stages, i.e. $\beta = \beta_1$ (see Li and Wierzbicki, 2010), the softening coefficient evolves in the way described in Fig. 3(a). The damage D starts to accumulate at the beginning of the deformation, but softening begins when $D = D_0$. Softening ends when $\beta = 0$ and $D = D_c$, after which the element is removed. Exponent m controls the non-linearity of the process. The evolution of β in the combined model is illustrated in Fig. 3(b) and the calculation procedure is described in Table 1. During the 1st stage $m_1 < 1$ describes the exponential reduction and during the second stage $m_2 \geqslant 1$ describes the logarithmic or linear reduction from the undamaged material curve. Individual softening stages can be shut off by setting $m = 0$; then β in Eq. (4) evolves according to Fig. 3(a).

2.4. Identification of softening parameters

The softening relation describing crack initiation and propagation in large shell elements is identified from the comparison with a detailed 3D model. Thereby, two FE models are required: a fine solid one and a coarse shell one. In both models, the strain energy density describes the local fracture process in the predefined volume V, referred to as representative volume element (RVE). In the shell model, an RVE corresponds to a single large element, while in the solid model it consists of several small elements. In a global sense, this averaging unit is located in the same position in both models. The strain energy density U, evaluated as the crack moves through the RVE, at every time increment t is:

$$U^t = \frac{\int_V \sigma_{ij}^t \varepsilon_{ij}^t dV^t}{\int_V dV^t}, \tag{6}$$

where σ_{ij} and ε_{ij} are the individual stress and strain components, respectively. The principle for comparing energies in the RVE is illustrated in Fig. 4.

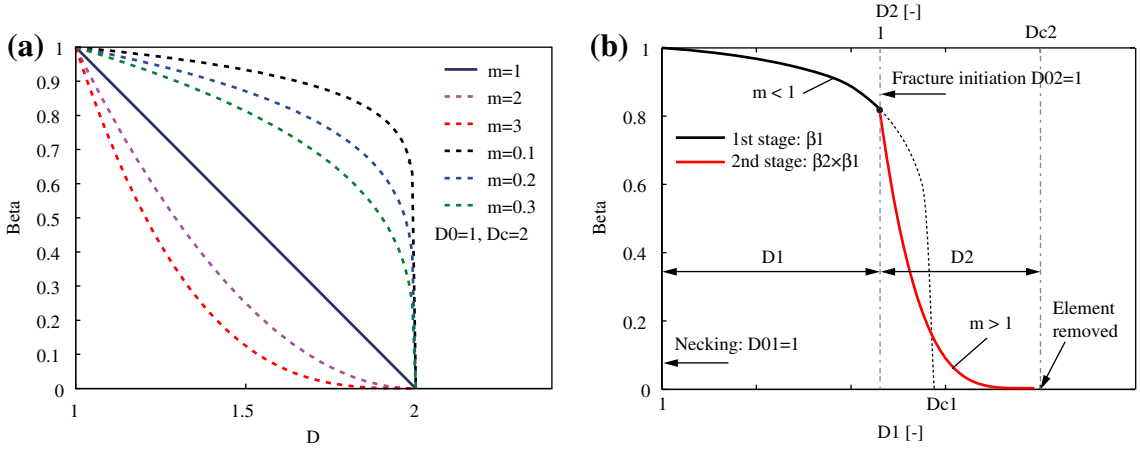

Fig. 3. Evolution of softening coefficient. (a) Only one softening stage considered (Figure from Li and Wierzbicki, 2010). (b) In the current model.

Table 1
Algorithm to calculate beta.

Damage parameters D_1 and D_2 are known from Eqs. (1) and (2). Compute β according to Eq. (4)

if $D_1 = 1$ **then** calculate critical damage value D_{c1} for the 1st stage
  $D_{c1} = D_2^{-1}$
end if
if there is necking, but no fracture: $D_1 \geqslant 1$ and $D_2 < 1$ **then**
  Calculate β_1 according to Eq. (5) using D_1, m_1 and D_{c1} and save as a state variable for the next increment
  Define β according to Eq. (4) whereas $\beta_2 = 1$, thus $\beta = \beta_1$
else if fracture criterion is satisfied, $D_2 \geqslant 1$ **then**
  Calculate β_2 according to Eq. (5) using D_2
  Define β according to Eq. (4): $\beta = \beta_1 \cdot \beta_2$
end if

3. Case study

3.1. Calibration with large-scale tearing experiment

The softening model is implemented into the commercial code ABAQUS/Explicit v6.11-2 as a user-defined material model (Appendix B). The numerical simulation results are validated with the previously published Mode I tearing experiments of 5-mm-thick normal-strength steel (NS) plates conducted by Simonsen and Törnqvist (2004). As the experiments were carried out under quasi-static conditions, the same conditions are assumed in the simulations. Three different element lengths were considered: 10, 30, and 50 mm. This allows the influence of the discretisation length on the softening relation to be determined.

3.2. Material description

The uniaxial true stress–strain curve of the material is described with the power law $\sigma = C(\varepsilon + \varepsilon_0)^n$, where C, n, and ε_0 are the coefficients of the power law. They are defined in Table 1, together with the rest of the material parameters. Material model follows standard rate-independent von Mises isotropic plasticity with strain hardening.

It was shown by Simonsen and Törnqvist (2004) that the stress triaxiality is almost constant during the deformation. Therefore, the fracture locus in Eq. (2) reduces to a constant fracture strain criterion and the equivalent plastic strain becomes a good measure of fracture ductility. In other words, D_2 depends only on the plastic strain. Furthermore, they found the following relation between the fracture strain, element length, and plate thickness t: $\bar{\varepsilon}_f^p = 0.5(L_e/t)^{-0.4}$. This relation is used here and the fracture strains for different element lengths are listed in Table 3.

Table 2
Material parameters.

Parameter	Notation	Value
Elastic modulus	E	210 GPa
Poisson ratio	v	0.3
Yield stress	σ_y	273 MPa
Power law coefficient 1	C	650 MPa
Power law coefficient 2	ε_0	0.01
Hardening exponent	n	0.23

Table 3
Fracture strains.

L_e	10	30	50
$\bar{\varepsilon}_f^p$	0.38	0.24	0.2

3.3. Experimental set-up

The details of the experimental set-up are shown in Fig. 5(a), together with the main testing variables that were simultaneously measured during the experiment; the crosshead load from the testing machine, P, and the crosshead displacement, δ. In the simulations, we assumed that the plate is ideally fixed to the test frame, although in the experiments some sliding might have occurred. The boundaries of the plate were forced to rotate about the pin-holes with a certain rotational velocity ω. The crosshead load P was calculated by knowing the time histories of the angle of rotation $\Delta\phi^i = \phi^i - \phi^{i-1}$ and external energy $\Delta E_{ext}^i = E_{ext}^i - E_{ext}^{i-1}$ applied to the system:

$$P^i = \frac{\Delta E_{ext}^i}{2L\sin(\Delta\phi^i)}, \tag{7}$$

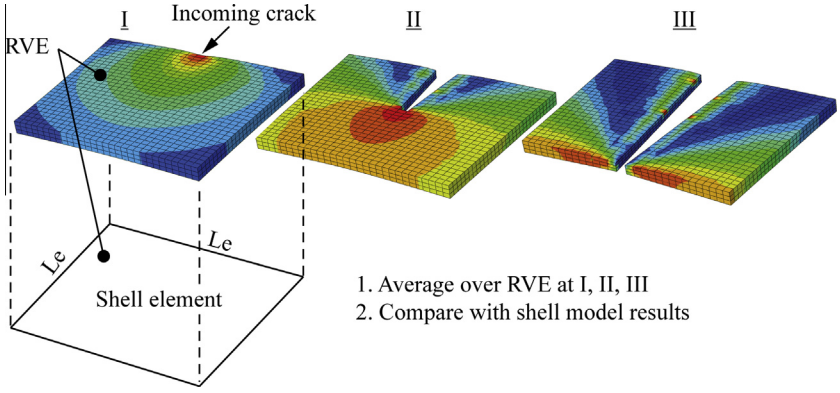

Fig. 4. Principle for comparing the solid and shell results in the RVE at different levels of deformation.

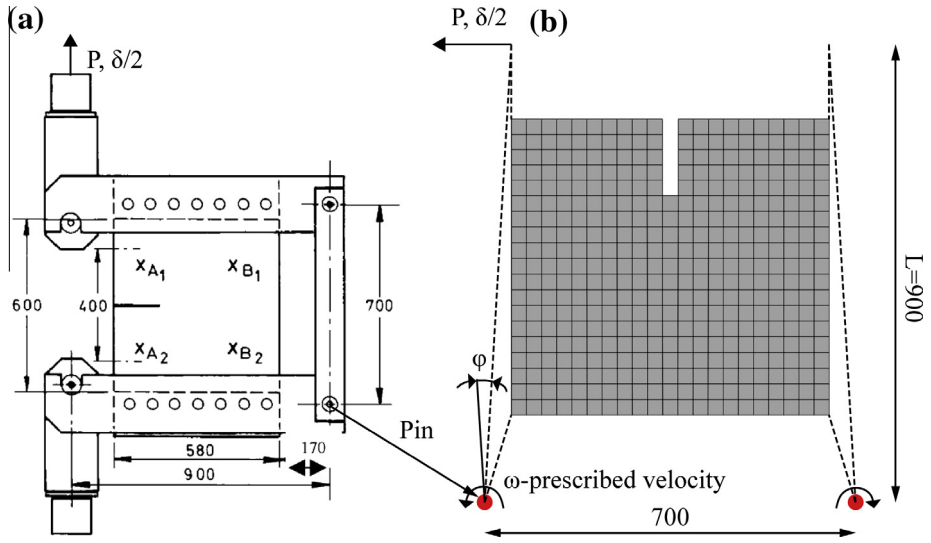

Fig. 5. (a) Experimental set-up of large-scale tearing experiment and (b) the FE interpretation.

where L is the length between the pin and the crosshead, and i is the time step index. The FE interpretation of the boundary conditions is shown in Fig. 5(b) for a shell element model with a 30-mm mesh size.

3.4. FE modelling

Detailed stress strain histories in the crack tip were obtained from the fine solid element model. Only half of the plate thickness was modelled by exploiting the symmetry of the plate geometry (out-of-plane translation and in-plane rotations fixed). In the thickness direction the element length is 0.83 mm. The in-plane dimensions along the expected crack path are 1×1 mm^2; outside this region a coarser mesh is used, with an approximate element length of 10 mm; see Fig. 6(a). The chosen mesh density might be too coarse to capture the whole crack tip mechanism. Nevertheless, in the context of the current analysis where strain energy density is averaged over the RVE, the detailed modelling of the crack tip behaviour is not necessary. The solid element is eight nodes with reduced integration (C3D8R). A constant fracture strain criterion ($\bar{\varepsilon}_f = 0.6$) was used in the simulations. The fracture strain was iterated until an excellent correspondence between the experimental and simulated surface crack extension and load–displacement curves was obtained.

All the shell element models were discretised with a four-node shell element with reduced integration (S4R) and 5 integration

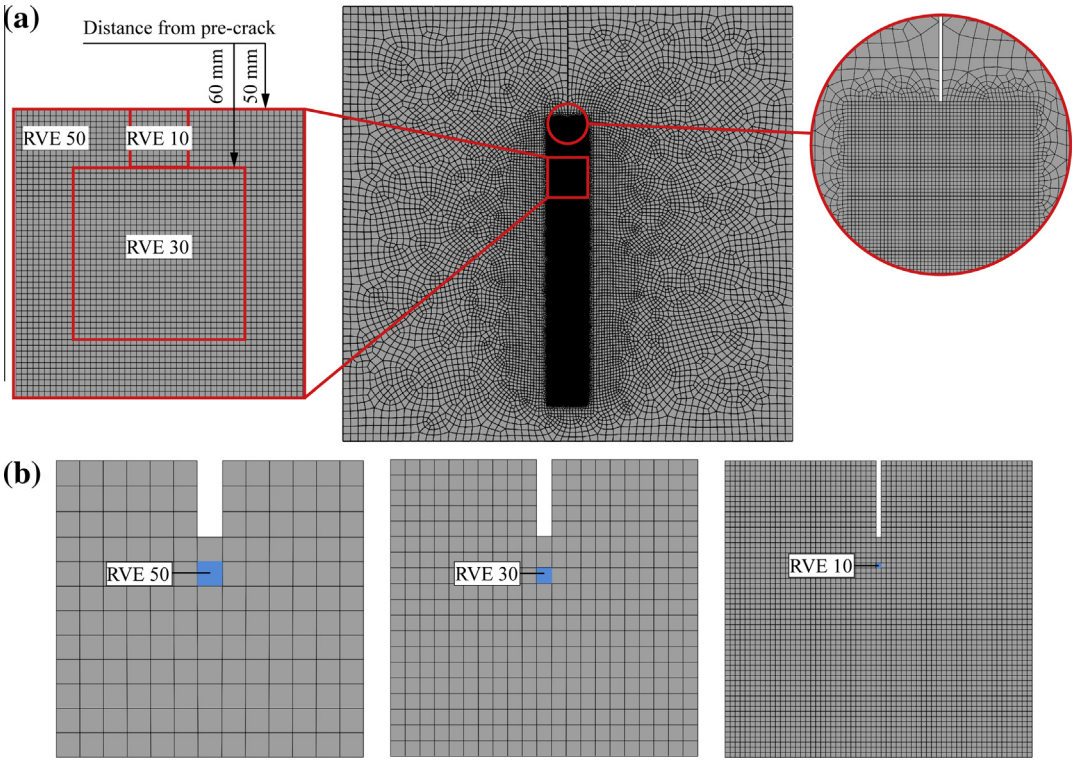

Fig. 6. (a) Solid and (b) shell FE models showing the locations of the RVE.

points through its thickness. The discretised models and the locations of RVE are shown in Fig. 6. The simulations were carried out with a sudden fracture criterion and the softening model formulated in this work. The fracture was simulated by removing the elements.

The relative displacement approach of ABAQUS (2011) used by Hogström et al. (2009) and AbuBakar and Dow (2013) was also employed to test the behaviour with a varying element length. This approach requires the strain at the beginning of softening $\bar{\varepsilon}_0^p$ and the critical displacement at fracture initiation: $u_f = \bar{\varepsilon}_f^p \times L_e$. This critical displacement is defined with the fracture strain in Table 2. Softening in Hogström et al. (2009) model begins at necking $\bar{\varepsilon}_0^p = n$, and in AbuBakar and Dow (2013) model at $\bar{\varepsilon}_0^p = 0.5\bar{\varepsilon}_f^p$. The evolution of the softening coefficient in these models is shown in Fig. 7.

Note that the fracture strain in the 50-mm elements is lower and in the 30-mm elements it is close to the hardening exponent, $n = 0.23$ (0.2 and 0.24, respectively). Thus, the 1st softening stage was started at a slightly lower equivalent strain value ($\bar{\varepsilon}^p = 0.15$) than dictated by the diffuse necking condition. Otherwise, the influence of the 1st softening stage on the simulation results cannot be determined. In Hogström et al. (2009) model the necking strain was changed in a similar way. The physical justification for using a lower necking strain is provided by the imperfections in the material, which are discarded in the analytical value (Li and Karr, 2009).

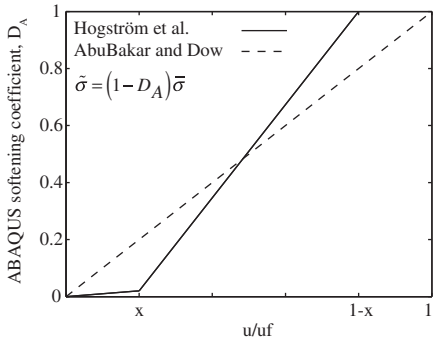

Fig. 7. Linear and bilinear softening law used in different studies. Here $x = 0.2$ is the calibration parameter defined by Hogström et al. (2009).

3.5. Softening relations

The softening parameters were first determined for the 30-mm elements. The basis for selection was the best fit between the solid and shell strain energy density distribution in the RVE; see Fig. 8(a). Table 4 contains the two sets of parameters chosen for the current model. In the first case, both softening stages were active, while in the second case, the 1st stage was shut off to see whether the necking portion of the softening curve is necessary at all. The resulting stress–strain histories in the RVE, i.e. the softening relations, are plotted in Fig. 8(b).

In Fig. 8(a), the peak in the strain energy density curve is understood as the point of fracture initiation in the RVE. As the crack propagates through the RVE in the solid model, the strain energy density U decreases correspondingly. The propagation stage cannot be predicted if large shell elements are removed suddenly. Nevertheless, the point of element removal corresponds almost perfectly with the displacement at complete failure of the RVE in the solid model. Correspondence is attained as the utilised fracture strains were calibrated on the basis of the crack extensions observed in the experiment (Simonsen and Törnqvist, 2004).

With softening, the crack propagation can be captured on the finite element level. The exception is AbuBakar and Dow (2013) model, which underestimates the energy density in RVE as softening begins too early. Because of that, their results are not discussed further in this section. Hogström et al. (2009) model yields the best correlation with the solid model during the propagation stage, but the peak value of the curve is slightly underestimated. The curves obtained with the current model are also very similar to the solid model results. This indicates that the 1st softening stage, describing necking, is not needed, as the crack propagation is the dominant mechanism governing the shape of the softening relation. This justifies the analysis employing only the 2nd stage, although in this case softening must begin before fracture strain is attained, i.e. $D_{02} = 0.8$; see Fig. 8(b).

Table 4
Softening parameters for 30-mm elements.

Description	D_{01}	m_1	D_{02}	m_2	D_{c2}
Current model: stages 1 and 2	1	0.1	0.99	1.5	1.6
Current model: only 2nd stage	–	0	0.8	1.5	1.6
Hogström et al. (2009)	$\bar{\varepsilon}_0^p = 0.15$, $\bar{\varepsilon}_f^p = 0.24$				
AbuBakar and Dow (2013)	$\bar{\varepsilon}_0^p = 0.12$, $\bar{\varepsilon}_f^p = 0.24$				

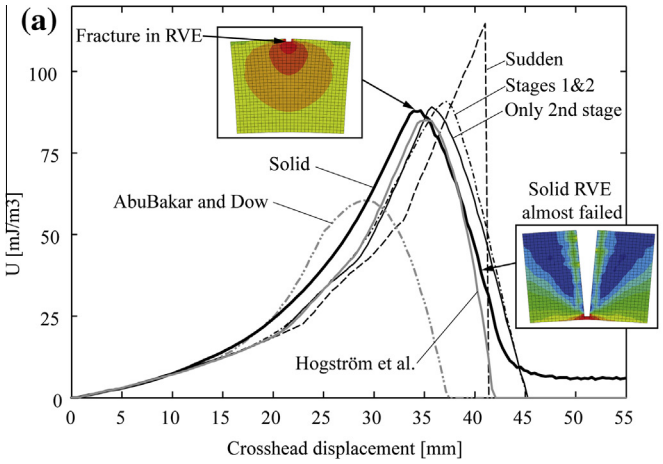

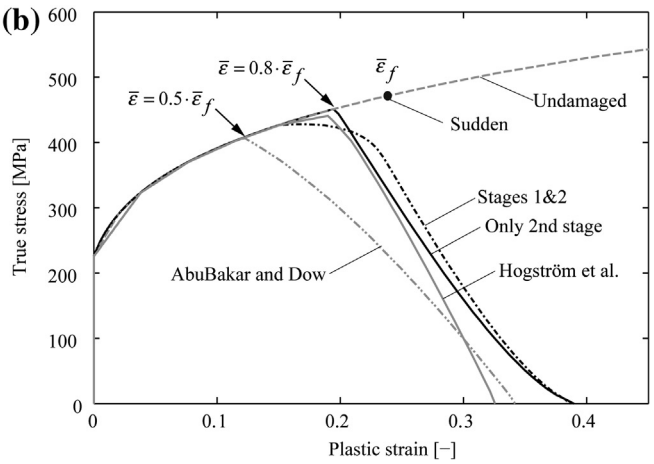

Fig. 8. Calibration of softening parameters. (a) Strain energy density U in the RVE. (b) Stress–strain history in the RVE.

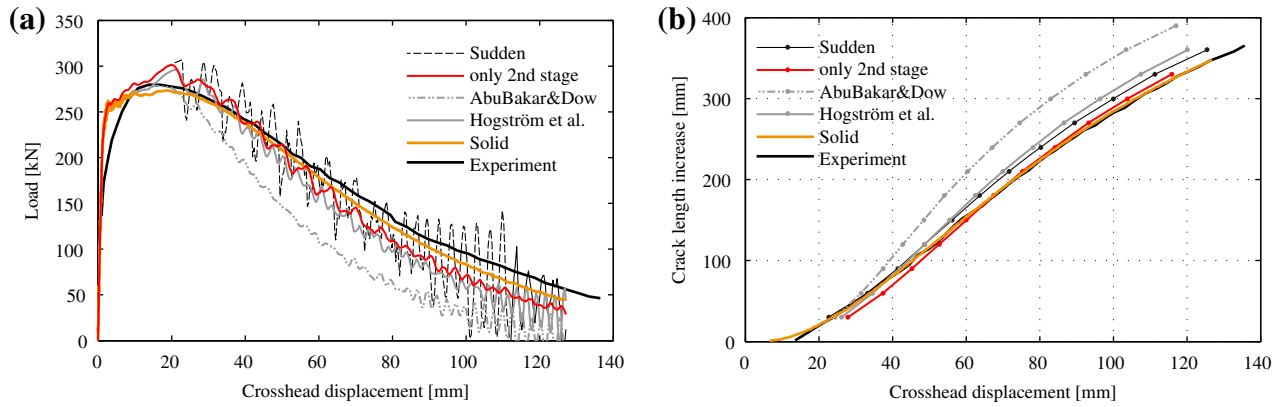

Fig. 9. Comparison of experimental and simulated curves. (a) Load–displacement curves. (b) Surface crack extension.

3.6. Simulation results

In Fig. 9(a), the experimentally measured load–displacement curve (Simonsen and Törnqvist, 2004) is compared with the FE simulation results. The solid simulation shows the best correspondence with the experiments. The distinct fluctuations in the 2D solution are associated with the sudden element removal and discontinuous growth pattern: stress is released when an element is removed, resulting in a drop in the load level. These fluctuations increase in amplitude during the final stages of the simulations since stress fields become more complex as a result of the reflection of stress waves from the plate boundary (Ren and Li, 2012). The oscillations are considerably reduced when the element stiffness decreases gradually. Fig. 9(b) shows that all the models, except that of AbuBakar and Dow (2013), can qualitatively predict the experimental crack length increase.

In the failure analyses of structures, crashworthiness is determined by the energy absorbed by the structure through plastic dissipation (Jones and Wierzbicki, 1983). Therefore, in Fig. 10 the normalised plastic dissipation energy in the whole structure, as well as in the RVE, is compared between different simulations. The best results locally in the RVE are obtained with the current softening model. This agreement also guarantees very good results in terms of the whole structure. With sudden element removal, the energy in the RVE is underestimated by about 15%, but at the structural level, the results agree almost perfectly with the solid simulation results. As expected, AbuBakar and Dow (2013) model again yields the most conservative estimate. At both levels, structural and RVE, Hogström et al. (2009) model underestimates the energy by about 10%.

The final fracture configurations are compared in Fig. 11. In a shell model without softening the stress contours in the crack tip are more similar to the solid model results. However, as indicated

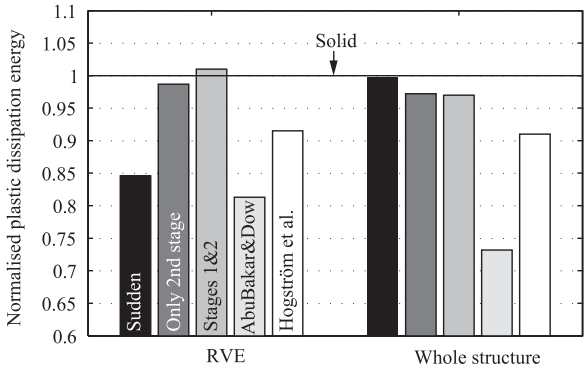

Fig. 10. Plastic dissipation energy.

by the strain energy density distributions in Fig. 8(a), on average the behaviour obtained with the softening model corresponds more closely to that observed in the solid model. Around the crack surface the stress contours predicted by the softening model are also more consistent with the solid model results. The phenomenon that takes place is similar to crack tip behaviour: after stress reduction in the element, deformation does not only move vertically along the crack tip into a neighbouring element, but also horizontally to the sides. In simulations without softening this does not happen.

3.7. Effect of mesh size

The softening parameters for the 10- and 50-mm elements were derived in the same way as for the 30-mm elements. They are presented in Table 4. The test simulations again showed that employ-

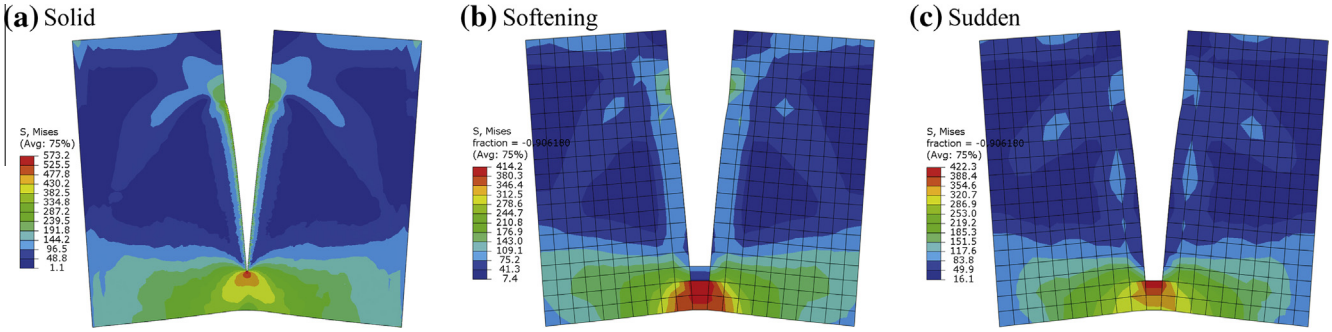

Fig. 11. Effective stress contours shown for three cases. (a) Solid model with 1-mm mesh. Shell models with 30-mm mesh: (b) with softening (current model, only 2nd stage); (c) without softening.

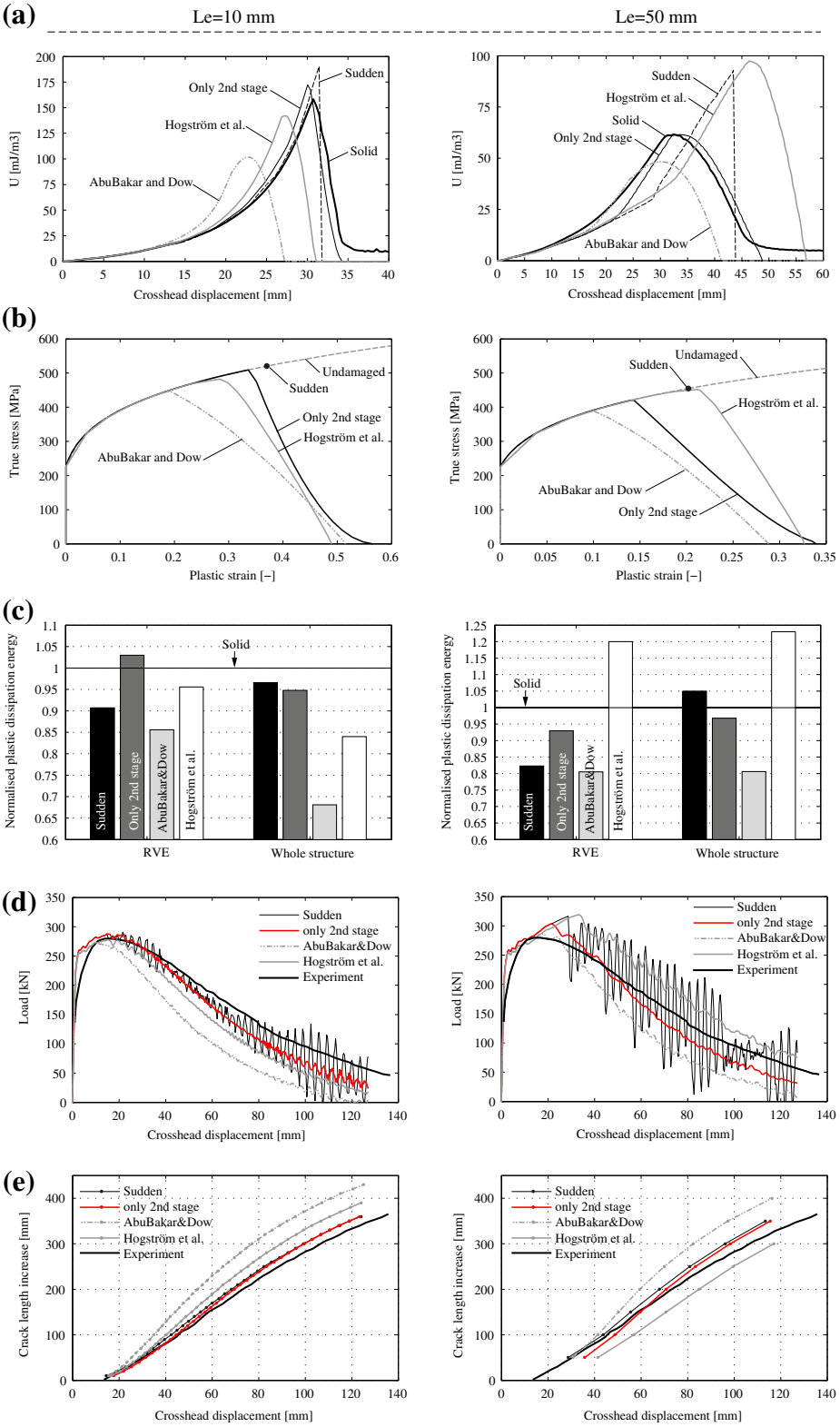

Fig. 12. Effect of mesh size. (a) Strain energy density U in RVE. (b) Stress–strain history in the RVE (–). (c) Plastic dissipation energy. (d) Load–displacement curves. (e) Surface crack extension curves.

ing the 1st softening stage is unnecessary, and thus only the results obtained with the 2nd stage are presented. The strain energy density distributions in Fig. 12(a) indicate the reason why the softening parameters had to be modified in the current model in comparison with the 30-mm case. In the models of Hogström et al. (2009) and AbuBakar and Dow (2013) the modification of the parameters is implicitly included: element size sensitivity is taken care of by the u_f-parameter, which is adjusted on the basis of the fracture strain. However, the curves do not match the 3D response. (See Table 5)

Table 5
Softening parameters for 10- and 50-mm elements.

Description	L_e	D_{01}	m_1	D_{02}	m_2	D_{c2}
Current model: only 2nd stage	10	–	0	0.9	2	1.5
Current model: only 2nd stage	50	–	0	0.7	1.5	1.7
	$L_e = 10$				$L_e = 50$	
Hogström et al. (2009)	$\bar{\varepsilon}_0^p = 0.24,\ \bar{\varepsilon}_f^p = 0.38$				$\bar{\varepsilon}_0^p = 0.15,\ \bar{\varepsilon}_f^p = 0.2$	
AbuBakar and Dow (2013)	$\bar{\varepsilon}_0^p = 0.5\bar{\varepsilon}_f^p,\ \bar{\varepsilon}_f^p = 0.38$				$\bar{\varepsilon}_0^p = 0.5\bar{\varepsilon}_f^p,\ \bar{\varepsilon}_f^p = 0.2$	

3.7.1. Plastic dissipation energy in Fig. 12(c)

With the current model the total plastic dissipation energy in the whole structure is accurately predicted with an error that is not larger than 5%. In the RVE, the results are the most accurate compared with the others. The sudden criterion yields similar results to the 30-mm element analysis: there is a relatively large error in RVE, but in the whole structure, the energy is accurately predicted. Hogström et al. (2009) model underestimates the total energy in the structure by 15% in the 10-mm elements and overestimates it by 23% in the 50-mm ones. The error given by AbuBakar and Dow (2013) model in the 10-mm elements is even larger, while in the 50-mm elements it is in the same range, but on the conservative side.

3.7.2. Load–displacement and crack extension

The crack extensions in Fig. 12(e) obtained with the current model and sudden criterion practically overlap. On average, they are also the same in the load–displacement curve in Fig. 12(d), but the oscillations are again considerably reduced; this is well exemplified by the 50-mm element results. The inability of the models of Hogström et al. (2009), and AbuBakar and Dow (2013) to correctly predict the total plastic dissipation energy is clearly present in the load–displacement and crack extension curves in Fig. 12(d) and (e).

4. Discussion

Analyses show that the successful prediction of fracture with large shell elements requires the careful calibration of the softening parameters. If the softening parameters are derived from the RVE by comparing strain energy density functions, both the fracture initiation and propagation can be characterised with large shell elements. Consequently, the dissipated plastic energy in the structure, the load–displacement curve, and the crack extension are captured with good accuracy. On the other hand, if the calibration is done on the basis of a tensile test (Woelke and Abboud, 2012; Hogström et al., 2009), the softening relation can correctly describe the material behaviour from necking only until fracture initiation. However, the 30-mm element simulations showed that fracture propagation in large shell elements is the dominant mechanism that determines the softening relation; see Fig. 8. Nevertheless, the point in the flow curve where the stress reduces to zero (fracture propagated through the element) predicted by the models of Hogström et al. (2009) and AbuBakar and Dow (2013) in all simulations is close to the one given by the current model; see Figs. 8(b) and 12(b). This is because of the relative displacement approach of ABAQUS, where the strain at element removal scales with element size. However, the reason why the results are not in alignment with the current model is that the point of fracture initiation, i.e. the beginning of softening, is not accurately predicted. In Hogström et al. (2009) model softening begins at necking, which gives a good estimate in 30-mm elements (Fig. 8(a)), but not in 10- and 50-mm elements (Fig. 12(a)). The assumption by AbuBakar and Dow (2013) of using half of the fracture strain measured from the tensile test is clearly too conservative. In the current model, the beginning of softening changes according to the element size: earlier in large elements $D_{02} = 0.7$ and later in small elements $D_{02} = 0.9$. The latter result is consistent with the analysis of Li and Wierzbicki (2010) with much smaller elements, where softening began at $D_{02} = 1$ (using the current notation). Simulations with the sudden criterion (Yamada et al., 2005; Simonsen and Törnqvist, 2004; Bao and Wierzbicki, 2004a; Törnqvist, 2003) showed an interesting tendency to underestimate the plastic energy dissipation in the RVE, while in the whole structure it was correctly captured. Moreover, the sudden criterion predicted the structural energy dissipation more accurately in all cases than the models of AbuBakar and Dow (2013) and Hogström et al. (2009). The accuracy of the current model in predicting the plastic dissipation energy in the whole structure is similar to that of the sudden criterion. Whether this remains valid under more complicated loading paths must be determined in a separate study.

5. Conclusion

In this paper, a numerical method for predicting softening parameters for large shell elements is presented. The basis for the method is the comparison of energy densities between the fine solid and coarse shell FE models as the crack propagates through the RVE. The simulation results clearly show that the softening model requires careful calibration and the separation of two distinct phenomena: fracture initiation and propagation. Without proper calibration, the results with the sudden fracture criterion provided a more accurate estimate in terms of the plastic energy dissipation in the structure. This fact should be considered when using softening in the analysis of large structures. Furthermore, the comparison of results with sudden fracture criterion suggests that the shape of the flow curve in the softening regime is not as critical as the total plastic work. This conclusion is similar to the one reached in Cohesive Zone Model studies. That is, the effect of traction-separation law on the fracture behaviour is limited, as long as total energy is correctly captured (Tvergaard and Hutchinson, 1992). This also explains why the 1st softening stage, describing necking, is not necessarily needed. On the other hand, the role of 1st stage might become more pronounced if the crack initiation under multi-axial stress state is considered. However, investigation of this is left for future.

With sudden criterion the plastic energy dissipated in the crack tip is always underestimated. In addition, the softening models remove discontinuity from the fracture propagation process. Still, the calibration of the softening parameters remains a challenging task. We realise that calibration by curve fitting the simulated and experimental results of a large tearing test is nearly impossible to conduct in general, and thus future work should outline a calibration procedure based on simpler approaches, e.g. CT specimens with full-field strain measurements.

Obviously, the results are valid for the current Mode I type of tearing case, which allowed assuming constant stress triaxiality during fracture propagation. In real structures such idealistic conditions rarely occur due to the changing load conditions and inconsistencies in structural arrangements in the form of stiffeners,

welds, notches etc. Under the various stress states and strain paths material ductility can change significantly as shown recently by Bao and Wierzbicki (2004b), Barsoum and Faleskog (2007), Haltom et al. (2013), Lou et al. (2012) and Korkolis and Kyriakides (2009). However, whether the fracture behaviour obtained with detailed analysis can be directly applied to large shell elements or should these results be appropriately scaled is out of the scope of this paper. This issue has been addressed by Walters and Schipperen (2012) and Choung et al. (2012). The virtue of limiting the study to a single stress state lies in the simplicity of interpreting the results with respect to modelling softening with large shell elements. Under more complicated conditions (stress states), contributions from different phenomena would be hard to separate. In that case, calibration should be based on carefully planned experiments in which the stress state under study is preserved at least in the range of RVE. Furthermore, the experiments should be supported by the detailed FE calculations. For instance, employing micro-mechanics based GTN model (Needleman and Tvergaard, 1984) including appropriate modifications for different stress states (Xue, 2008; Nahshon and Hutchinson, 2008).

Acknowledgements

First author was supported by the Graduate School of Engineering Mechanics, funded by the Finnish Academy of Sciences. This is gratefully acknowledged. Thanks are due to Dr. Kristjan Tabri and Ingrit Lillemäe for proof reading the article. Appreciation is also due to CSC – IT Centre for Science Ltd. for providing ABAQUS software license. Special thanks goes to Dr. Heikki Remes for providing valuable suggestions during revision process.

Appendix A

The condition for diffuse necking according to the Considère construction is stated as follows (Rees, 2006):

$$\frac{1}{\bar{\sigma}}\frac{d\bar{\sigma}}{d\bar{\varepsilon}} = 1. \tag{A.1}$$

Under the assumption of power law hardening, $\bar{\sigma} = C\bar{\varepsilon}^n$ (where C is the strength coefficient and n is the strain hardening exponent), the diffuse necking condition (A.1) can be expressed in terms of strain:

$$\frac{1}{\bar{\sigma}}\frac{d\bar{\sigma}}{d\bar{\varepsilon}} = \frac{C\cdot n\cdot \bar{\varepsilon}^{n-1}}{C\bar{\varepsilon}^n} = \frac{n}{\bar{\varepsilon}} = 1. \tag{A.2}$$

Appendix B

Constitutive. equations

The material model with softening is implemented into the commercial code ABAQUS/Explicit using VUMAT subroutines as a user-defined material model. The constitutive equations based on small deformation, rate-independent von Mises isotropic plasticity with strain hardening are coupled with the softening coefficient β; see also (Andrade Pires et al., 2004; Xue, 2007). Elastic predictor, plastic corrector (return mapping) scheme, is used to numerically integrate elastoplastic constitutive equations, see (De Souza Neto et al., 2008; Hallquist, 2006).

In this formulation the total strain tensor is decomposed into elastic and plastic parts:

$$\varepsilon_{ij} = \varepsilon^e_{ij} + \varepsilon^p_{ij}. \tag{B.1}$$

On the basis of the hypothesis of strain equivalence, the elastic softened (trial) stress tensor is:

$$\tilde{\sigma}_{ij} = \tilde{\lambda}\delta_{ij}\varepsilon^e_{kk} + 2\tilde{\mu}\varepsilon^e_{ij}, \tag{B.2}$$

or in Jaumann corotational rate form:

$$\tilde{\sigma}^J_{ij} = \tilde{\lambda}\delta_{ij}\dot{\varepsilon}^e_{kk} + 2\tilde{\mu}\dot{\varepsilon}^e_{ij}, \tag{B.3}$$

where δ_{ij} is the Kronecker delta and $\tilde{\lambda}$ and $\tilde{\mu}$ are Lame's constants resulting from the softened elastic modulus $\tilde{E}$:

$$\tilde{E} = \beta E_0 \tag{B.4}$$

where E_0 is the initial undamaged elastic modulus and β is the softening coefficient calculated with Eq. (4). Therefore, the elastic modulus decreases at the same rate. The Poisson's ratio is assumed to remain constant throughout the damaging process. Material yields according to von Mises yield function:

$$f = \sqrt{\frac{3}{2}\tilde{s}_{ij}\tilde{s}_{ij}} - \beta[\sigma_{y0} + R(\bar{\varepsilon}^p)] = 0\begin{cases}\leqslant 0 \text{ for elastic or neutral loading}\\ > 0 \text{ for plastic hardening,}\end{cases} \tag{B.5}$$

where $\tilde{s}_{ij}$ is the deviatoric part of the stress tensor calculated with Eq. (B.2), σ_{y0} is the initial yield strength of the undamaged material, and R is the isotropic hardening function depending on accumulated plastic strain. Note that in Eq. (B.5) effect of softening upon the plastic behaviour is accounted for by using damaged deviatoric stress tensor, instead of undamaged tensor s_{ij}. If the elastic trial stress given with Eq. (B.3) satisfies the yield function nothing else is done and the stress update is purely elastic. Otherwise, if the material starts to yield, the rate of equivalent plastic strain is calculated

$$\dot{\bar{\varepsilon}}^p_{ij} = \sqrt{\frac{2}{3}\dot{\varepsilon}^p_{ij}\dot{\varepsilon}^p_{ij}}, \tag{B.6}$$

where $\dot{\varepsilon}^p_{ij}$ is the plastic strain increment. From the associative von Mises flow rule

$$\dot{\varepsilon}^p_{ij} = \dot{\bar{\varepsilon}}^p_{ij}\sqrt{\frac{3}{2}}\frac{s_{ij}}{\|s_{ij}\|}. \tag{B.7}$$

References

ABAQUS, 2011. ABAQUS Analysis User's Manual, Version 6.11, Dassault Systèmes Simulia Corporation.
AbuBakar, A., Dow, R.S., 2013. Simulation of ship grounding damage using the finite element method. Int. J. Solids Struct. 50 (5), 623–636.
Alsos, H.S., Hopperstad, O.S., Törnqvist, R., Amdahl, J., 2008. Analytical and numerical analysis of sheet metal instability using a stress based criterion. Int. J. Solids Struct. 45 (7–8), 2042–2055.
Andrade Pires, F.M., De Souza Neto, E.A., Owen, D.R.J., 2004. On the finite element prediction of damage growth and fracture initiation in finitely deforming ductile materials. Comput. Methods Appl. Mech. Eng. 193 (48–51), 5223–5256.
Bao, Y., Wierzbicki, T., 2004a. A comparative study on various ductile crack formation criteria. J. Eng. Mater. Technol. 126 (3), 314.
Bao, Y., Wierzbicki, T., 2004b. On fracture locus in the equivalent strain and stress triaxiality space. Int. J. Mech. Sci. 46 (1), 81–98.
Barsoum, I., Faleskog, J., 2007. Rupture mechanisms in combined tension and shear – experiments. Int. J. Solids Struct. 44 (6), 1768–1786.
Besson, J., 2010. Continuum models of ductile fracture: a review. Int. J. Damage Mech. 19 (1), 3–52.
Chaboche, J.-L., 1981. Continuous damage mechanics – a tool to describe phenomena before crack initiation. Nucl. Eng. Des. 64 (2), 233–247.
Choung, J., Shim, C.-S., Song, H.-C., 2012. Estimation of failure strain of EH36 high strength marine structural steel using average stress triaxiality. Mar. Struct. 29 (1), 1–21.
De Souza Neto, E.A., Peric, D., Owen, D.R.J., 2008. Computational Methods for Plasticity: Theory and Applications, first ed. Wiley.
Gruben, G., Hopperstad, O.S., Børvik, T., 2012. Simulation of ductile crack propagation in dual-phase steel. Int. J. Fract. 180 (1), 1–22.
Hallquist, J.O., 2006. LS-Dyna Theory Manual. Livermore Software Technology Corp., Livermore.
Haltom, S.S., Kyriakides, S., Ravi-Chandar, K., 2013. Ductile failure under combined shear and tension. Int. J. Solids Struct. 50 (10), 1507–1522.
Hogström, P., Ringsberg, J.W., 2012. An extensive study of a ship's survivability after collision – a parameter study of material characteristics, non-linear FEA and damage stability analyses. Mar. Struct. 27 (1), 1–28.

Hogström, P., Ringsberg, J.W., Johnson, E., 2009. An experimental and numerical study of the effects of length scale and strain state on the necking and fracture behaviours in sheet metals. Int. J. Impact Eng. 36 (10–11), 1194–1203.

Jones, N., 2013. The credibility of predictions for structural designs subjected to large dynamic loadings causing inelastic behaviour. Int. J. Impact Eng. 53, 106–114.

Jones, N., Wierzbicki, T., 1983. Structural Crashworthiness. Butterworth & Co (Publishers) Ltd.

Korkolis, Y.P., Kyriakides, S., 2009. Path-dependent failure of inflated aluminum tubes. Int. J. Plasticity 25 (11), 2059–2080.

Lemaitre, J., 1985. A continuous damage mechanics model for ductile fracture. J. Eng. Mater. Technol. 107 (1), 83.

Li, H., Fu, M.W., Lu, J., Yang, H., 2011. Ductile fracture: experiments and computations. Int. J. Plasticity 27 (2), 147–180.

Li, Y., Karr, D.G., 2009. Prediction of ductile fracture in tension by bifurcation, localization, and imperfection analyses. Int. J. Plasticity 25 (6), 1128–1153.

Li, Y., Wierzbicki, T., 2010. Prediction of plane strain fracture of AHSS sheets with post-initiation softening. Int. J. Solids Struct. 47 (17), 2316–2327.

Lou, Y., Huh, H., Lim, S., Pack, K., 2012. New ductile fracture criterion for prediction of fracture forming limit diagrams of sheet metals. Int. J. Solids Struct. 49 (25), 3605–3615.

Nahshon, K., Hutchinson, J.W., 2008. Modification of the Gurson model for shear failure. Eur. J. Mech. A Solid. 27 (1), 1–17.

Needleman, A., Tvergaard, V., 1984. An analysis of ductile rupture in notched bars. J. Mech. Phys. Solids 32 (6), 461–490.

Rees, D., 2006. Basic Engineering Plasticity: An Introduction with Engineering and Manufacturing Applications, first ed. Butterworth–Heinemann.

Ren, B., Li, S., 2012. Modeling and simulation of large-scale ductile fracture in plates and shells. Int. J. Solids Struct. 49 (18), 2373–2393.

Simonsen, B.C., Törnqvist, R., 2004. Experimental and numerical modelling of ductile crack propagation in large-scale shell structures. Mar. Struct. 17 (1), 1–27.

Teng, X., 2008. Numerical prediction of slant fracture with continuum damage mechanics. Eng. Fract. Mech. 75 (8), 2020–2041.

Törnqvist, R., 2003. Design of Crashworthy Ship Structures. Doctoral Thesis. DTU.

Tvergaard, V., Hutchinson, J.W., 1992. The relation between crack growth resistance and fracture process parameters in elastic–plastic solids. J. Mech. Phys. Solids 40 (6), 1377–1397.

Walters, C.L., Schipperen, J.H.A., 2012. The effect of mesh size on failure for shell structures. In: Proceedings of the International Crashworthiness Conference, iCrash 2012, Milan, Italy, July 18–20.

Woelke, P.B., Abboud, N.N., 2012. Modeling fracture in large scale shell structures. J. Mech. Phys. Solids 60 (12), 2044–2063.

Xue, L., 2008. Constitutive modeling of void shearing effect in ductile fracture of porous materials. Eng. Fract. Mech. 75 (11), 3343–3366.

Xue, L., 2007. Damage accumulation and fracture initiation in uncracked ductile solids subject to triaxial loading. Int. J. Solids Struct. 44 (16), 5163–5181.

Yamada, Y., Endo, H., Pedersen, P.T., 2005. Numerical study on the effect of buffer bow structure in ship-to-ship collisions. In: Proceedings of the 15th (2005) International Offshore and Polar Engineering Conference (ISOPE), Seoul, Korea, June 19–24, 2005.